IEEE Access
Multidisciplinary : Rapid Review : Open Access Journal

Received October 12, 2021, accepted October 17, 2021, date of publication October 19, 2021, date of current version October 27, 2021.

Digital Object Identifier 10.1109/ACCESS.2021.3121411

Position Error Compensation of Façade-Cleaning Robot by Optimal Rope Winch Design

HONGJOON KYONG[1], MYEONGJIN CHOI[2], YECHEOL MOON[2], KYUNGWOOK LEE[2], JONGWON KIM[1], TAEGYUN KIM[3], AND TAEWON SEO[2], (Senior Member, IEEE)

[1]Department of Mechanical Engineering, Seoul National University, Seoul 08826, South Korea
[2]School of Mechanical Engineering, Hanyang University, Seoul 04763, South Korea
[3]School of Mechanical Engineering, Yeungnam University, Gyeongsan 38541, South Korea

Corresponding authors: Taegyun Kim (tgkim@yu.ac.kr) and Taewon Seo (taewonseo@hanyang.ac.kr)

This research was supported by the National Research Foundation of Korea (NRF) Grant funded by the Ministry of Science and ICT for First-Mover Program for Accelerating Disruptive Technology Development under Grants 2018M3C1B9088331, 2018M3C1B9088332, and Bridge Convergence R&D Program Grants 2021M3C1C3096807, 2021M3C1C3096808, and in part by the 2020 Yeungnam University Research Grant.

ABSTRACT This study aimed to optimize the rope winch of a façade-cleaning robot, a system that travels vertically using the friction between ropes and pulleys. However, position errors can be caused by various factors during locomotion. This adversely affects the robot's position accuracy. To solve this problem, an experiment was conducted to secure the repeatability of the robot position by optimizing it using the Taguchi method. Subsequently, an error compensation was designed by predicting slip errors of the rope, and accordingly the positional accuracy was determined through feedforward and feedforward + PI control. The experimental optimization confirmed that optimal repeatability can be obtained using a pressure module with the force of 45 N and an axial groove pitch angle of 6° of a pulley. The position accuracy was improved using an error prediction model based on weights, travel distances, and controllers. For a travel distance of 3.0 m, the position error could be reduced to 55%–81% and 72%–89% through feedforward control and feedforward + PI control, respectively, compared with that of the open-loop. The observations of this study could facilitate the control of the position of façade-cleaning robots and aid in the improvement of position accuracy.

INDEX TERMS Rope winch, position accuracy, position repeatability, rope position error modeling, differential gear mechanism.

NOMENCLATURE

$\dot{m}$	Rope mass flow rate (kg/s)
P	Mass per unit volume (kg/m^3)
$A(s)$	Area of the rope at position s (mm^2)
$v(s)$	Velocity of the rope at position s (m/s)
T	Tension of the rope (N)
dT	Differential Tension (N)
f	Projections of the force per unit length from the pulley on the rope in the tangential directions (N/m)
r	Radius of pulley (mm)
$d\theta$	Differential angle (rad)
ds	Differential location (m)
dv	Differential velocity (m/s)
n	Projections of the force per unit length from the pulley on the rope in the normal directions (N/m)
$T(s)$	Tension in the rope at position s
T_{ref}	Reference tension (N)
k	Stiffness of rope (N)
$\varepsilon(s)$	Strain of rope at position s
v_{ref}	Reference velocity (m/s)
T_{left}	Tension of left pulley (N)
T_{right}	Tension of right pulley (N)
M_{motor}	Motor torque (Nm)
T_1	Tension of right pulley after slip zone (N)
T_2	Tension of the mid part (N)
T_3	Tension of left pulley before slip zone (N)
$f_{ascend,left}$	Projections of the friction force per unit length on the left pulley while ascending (N/m)
$f_{ascend,right}$	Projections of the friction force per unit length on the right pulley while ascending (N/m)
ω_{left}	Angular velocity of left pulley (rad/s)
ω_{right}	Angular velocity of right pulley (rad/s)

The associate editor coordinating the review of this manuscript and approving it for publication was Agustin Leobardo Herrera-May.

This work is licensed under a Creative Commons Attribution 4.0 License. For more information, see https://creativecommons.org/licenses/by/4.0/

μ	Friction coefficient between rope and pulley
$\theta_{slip,left,ascend}$	Slip angle of the left pulley while ascending (rad)
$\theta_{slip,right,ascend}$	Slip angle of the right pulley while ascending (rad)
$\theta_{slip,left,descend}$	Slip angle of the left pulley while descending (rad)
$\theta_{slip,right,descend}$	Slip angle of the right pulley while descending (rad)
ε	Strain of the rope
E	Elasticity of the rope (N/mm^2)
A	Area of the rope (mm^2)
$d\delta_{slip}$	Differential rope deformation length at slip zone (m)
δ_{slip}	Rope deformation length at slip zone (m)
$\delta_{slip,ascend}$	Rope deformation length at slip zone while ascending (m)
$\delta_{slip,descend}$	Rope deformation length at slip zone while descending (m)

I. INTRODUCTION

Skyscrapers with a height of over 150 m exist worldwide [1]. These buildings are typically managed by human workers using a single rope or a building gondola. This can endanger the workers and even result in fatal injuries or death. According to the International Window Cleaning Association, at least one high-rise window cleaner died each year between 2010 and 2014 [2].

Many researchers have introduced and exploited different types of façade-cleaning robots (FCRs) to replace human workers in such cases. The TITO500, SIRIUSc, and CAFE robots can shift upward and downward using a crane located at the top of the building [3]–[5]. The building façade maintenance robot (BFMR) system requires the installation of a built-in rail on a building, and this can be used by the robots to climb up and down [6]. In addition, temporary equipment for climbing robots has been developed. KITE and SkyScraper-I utilize a gantry that is pinned on a building vertex [7], [8]. However, the installation of an additional gantry outside the building is a challenging and time-consuming process.

FCR Module 1 (FCR-M1) moves back and forth utilizing a building gondola; this platform can be used only if gondolas exist on the building [9].

Mobile-type cable-driven robots have also been developed. These have built-in winches and cables. Wall robots can shift upward and downward using a built-in winch and steel cable connected to the top of the roof [10]. However, the built-in winch system increases the weight of the robots, which, in turn, results in higher power consumption.

The Integrated Professional Cleaning Eagle Corporation (IPC Eagle) developed a free-end-type winch-steel cable system [11], in which, because the cable bundle is installed outside the robot, its payload is not influenced by the building height. However, the taller the skyscraper, the heavier is the steel cable. This hinders the installation of a rope bundle. In addition, the steel cable can damage the building's windows or columns because of the weight of the cable.

A single pulley-type winch was developed in a previous study to conveniently install devices on various types of buildings. It requires only one synthetic fiber rope, which is fixed at the top of the building. The winch was installed on the robotic platform of the wall-cleaning robot (ROPE RIDE) in a previous study [12]. However, the position accuracy was inadequate because of the slip and lift weights were limited by the low payload capacity.

A double traction winch is a system that utilizes two drums. Each drum has grooves to prevent the rope from slipping [13]. However, because the load is not distributed, the force is concentrated on the drums. Furthermore, the production cost increases because precision machining is required for the drum.

The cable traction control unit (CTCU) is a multipulley-type winch with a synthetic fiber rope and is employed for installing deep-sea structures. This system divides the load between pulleys to prevent their breakage. In addition, slip caused by rope elongation can be compensated for by controlling the speed of the pulleys [14]. Although this system may appear as an effective FCR rope winch, a number of motors are needed to control each pulley, resulting in a complex system.

A multi-wound differential pulley winch (MWDPW) has been proposed to improve position accuracy (Fig. 1, (b)) [15]. In this system, two pulleys and a differential gear module are installed at the center. The differential gear module uniformly distributes the torque applied on the pulleys, thereby preventing force concentration. In addition, because the MWDPW requires only a rope that is fixed on the roof, it can be installed conveniently on buildings.

Because MWDPW is driven by the friction between the pulley and rope, errors are caused by various factors, such as rope elasticity, loss of friction between rope and pulley, and backlash when the movement direction varies.

The length of the rope was utilized to estimate the position. Reduced position accuracy would hinder the accurate measurement of rope length, thereby causing difficulties in controlling the robot [16]. In addition, the application of a force higher than that intended on a building wall, owing to the position deviation, could damage weak wall materials such as glass panels [17].

Therefore, in this study, the Taguchi method was used to optimize position repeatability and secure the position accuracy of MWDPW by using error compensation. Optimal design parameters were determined by the experiments and the sensitivity analysis. Based on the optimal design parameters, the position error prediction model was applied through feedforward and feedforward + PI controller to minimize position errors.

The remainder of this paper is organized as follows. An error prediction model is introduced in Section 2.

In Section 3, test benches are introduced, and experiments are performed using the Taguchi method to secure position repeatability. Section 4 presents the experiments used to measure the rope modulus of elasticity and backlash as well as those conducted to verify that the position accuracy is improved using an error prediction model. The conclusions are presented in Section 5.

II. POSITION ERROR PREDICTION MODELING

A. ROPE AND PULLEY MECHANICS

A free body diagram of the rope and pulley was developed as shown in Fig. 2. It shows a portion of the rope of length ds at the location s and subtending an angle of $d\theta$. The Eulerian formulation was adopted to assume that the conditions at s are independent of time. Symbol ρ represents the mass per unit volume of the rope, $A(s)$ indicates the cross-sectional area of the rope, and $v(s)$ denotes the velocity of the rope's movement. The mass flow rate of the rope is assumed to be constant [18].

$$\dot{m} = \rho A(s)\, v(s) = constant \tag{1}$$

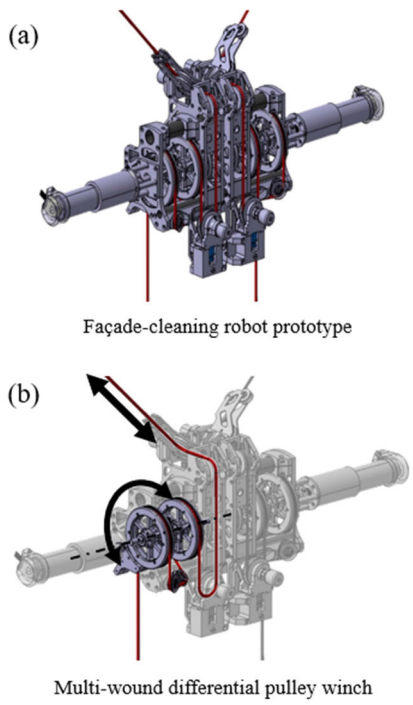

FIGURE 1. Schematics of the prototype of the façade-cleaning robot (a), Multi-wound differential pulley winch (b).

The directions of friction force $f(s)$ and normal direction force $n(s)$ (see Fig. 2) were set as positive counterclockwise and outward, respectively. The conservation of momentum projected in the tangential and normal directions is as follows:

$$\begin{aligned} &-T\cos\left(\frac{d\theta}{2}\right) + (T+dT)\cos\left(\frac{d\theta}{2}\right) - frd\theta, \\ &= \dot{m}dv\cos d\theta \end{aligned} \tag{2}$$

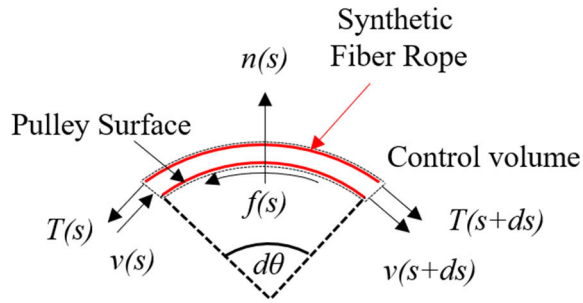

FIGURE 2. Free body diagram of a section of rope on a pulley.

$$\begin{aligned} &-T\sin\left(\frac{d\theta}{2}\right) - (T+dT)\sin\left(\frac{d\theta}{2}\right) + nds \\ &= -\dot{m}v\sin\left(\frac{d\theta}{2}\right) - \dot{m}(v+dv)\sin\left(\frac{d\theta}{2}\right). \end{aligned} \tag{3}$$

Assuming that $d\theta \ll 1$, $\cos(d\theta/2) \fallingdotseq 1$, and $\sin(d\theta/2) \fallingdotseq d\theta/2$, (2) and (3) are reduced to

$$dT - fds = \dot{m}dv, \tag{4}$$

$$n = \frac{T - \dot{m}v}{r}. \tag{5}$$

The rope is deformed because of the variation in its tension. Therefore, an additional equation is required for the tension and tensile force. The rope is assumed to be linearly elastic and that the rope tension at any point s is as follows:

$$T(s) = T_{ref} + k\varepsilon(s), \tag{6}$$

where k represents the stiffness (N) and T_{ref} denotes the tension at the reference point. Furthermore, strain $\varepsilon(s)$ at any point is associated with the velocity of the rope. The velocity of the rope in the reference state is expressed as follows:

$$v(\mathrm{s}) = v_{ref}(1 + \varepsilon(s)). \tag{7}$$

The tension can be expressed as a function of the rope speed. Assuming $T_{ref} = 0$ and combining (6) and (7),

$$T(\mathrm{s}) = k\left(\frac{v(s)}{v_{ref}} - 1\right) \tag{8}$$

A slip zone is developed when differences in tension occur between the entry and exit ends of the rope. The slip zone produced on both the pulleys is presented in Fig. 3. Furthermore, the tension is assumed to be constant otherwise. The rope deforms owing to differences in tension within the slip zone. This, in turn, causes positioning error of the robot [15], [19].

B. TENSION ACTING ON THE PULLEY WHILE ASCENDING

It is assumed that the torque transferred to the pulley is distributed equally owing to the differential gear mechanism. Therefore, the motor torque distributed to both the pulleys can be expressed as follows:

$$T_{left} = \frac{M_{motor}}{2r} - (T_3 - T_2), \tag{9}$$

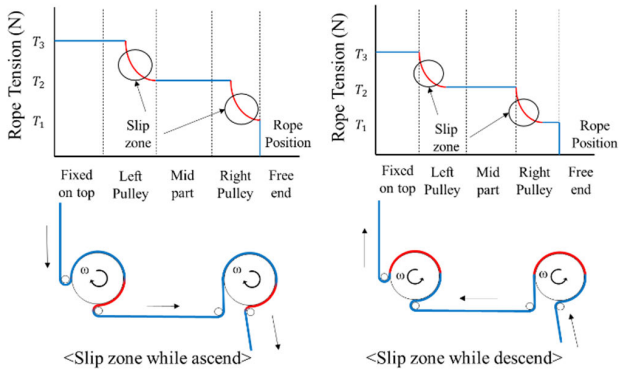

FIGURE 3. Schematic of rope winch slip zone.

$$T_{right} = \frac{M_{motor}}{2r} - (T_2 - T_1). \tag{10}$$

Combining (8) with (9) and (10)

$$T(s) = T_{left} = \frac{M_{motor}}{2r} - (T_3 - T_2) = k\left(\frac{r\omega_{left}}{v_{ref}} - 1\right), \tag{11}$$

$$T(s) = T_{right} = \frac{M_{motor}}{2r} - (T_2 - T_1) = k\left(\frac{r\omega_{right}}{v_{ref}} - 1\right), \tag{12}$$

$$v_{ref} = k\left(\frac{r\omega_{left}}{\frac{M_{motor}}{2r} - (T_3 - T_2) + k}\right), \tag{13}$$

$$v_{ref} = k\left(\frac{r\omega_{right}}{\frac{M_{motor}}{2r} - (T_2 - T_1) + k}\right). \tag{14}$$

By combining (11)–(14)

$$T(\mathrm{s}) = \left(\frac{v(s)}{r\omega_{left}}\left(\frac{M_{motor}}{2r} - (T_3 - T_2) + k\right) - k\right), \tag{15}$$

$$T(\mathrm{s}) = \left(\frac{v(s)}{r\omega_{right}}\left(\frac{M_{motor}}{2r} - (T_2 - T_1) + k\right) - k\right). \tag{16}$$

1) NON-SLIP ZONE OF LEFT PULLEY

The tension of the rope and velocity in the nonslip zone were assumed to be constant.

$$dT = dv = 0, \quad f(s) = 0 \tag{17}$$

$$T(s) = T_{left} = \frac{M_{motor}}{2r} - (T_3 - T_2) \tag{18}$$

$$v(s) = r\omega_{left}, \quad n(s) = \frac{T_{left} - \dot{m}r\omega_{left}}{r} \tag{19}$$

2) SLIP ZONE OF LEFT PULLEY

The direction of the friction force while ascending was assumed to be counterclockwise. The equations are summarized as follows based on (1)–(5):

$$f_{ascend,left} = \mu n, \tag{20}$$

$$\frac{dT - \dot{m}dv}{T - \dot{m}v} = \mu d\theta, \tag{21}$$

The integration of (21) over the entire slip zone yields

$$\theta_{slip,left,ascend} = \frac{1}{\mu}\ln\left(\frac{T(s) - \dot{m}v(s)}{T_{left} - \dot{m}r\omega_{left}}\right), \tag{22}$$

$$T(s) - \dot{m}v(s) = \left(\frac{M_{motor}}{2r} - (T_3 - T_2) - \dot{m}r\omega_{left}\right) \times e^{\mu\theta_{slip,left,ascend}}, \tag{23}$$

where $\theta_{slip,left,ascend}$ is defined as the division of the distance of the slip zone and the radius of the pulley. By combining (15) with (23) and assuming $X = \frac{M_{motor}}{2r} - (T_3 - T_2) - \dot{m}r\omega_{left}$

$$T(s) = \left[X + \frac{\dot{m}r\omega_{left}X}{(X+k)}\right]e^{\mu(\mathrm{s/r})} + \frac{\dot{m}r\omega_{left}k}{(X+k)}. \tag{24}$$

3) NONSLIP ZONE OF THE RIGHT PULLEY

Similar to the case of the left pulley, the tension of the rope and the velocity within the nonslip zone remained constant.

$$\mathrm{dT} = \mathrm{d}v = 0, \quad f(s) = 0 \tag{25}$$

$$T(s) = T_{right} = \frac{M_{motor}}{2r} - (T_2 - T_1) \tag{26}$$

$$v(s) = r\omega_{right}, \quad n(s) = \frac{T_{right} - \dot{m}r\omega_{right}}{r} \tag{27}$$

4) SLIP ZONE OF THE RIGHT PULLEY

The equations are developed similar to the previous case.

$$f_{ascend,right} = \mu n \tag{28}$$

$$\theta_{slip,right,ascend} = \frac{1}{\mu}\ln\left(\frac{(T(s) - \dot{m}v(s))}{T_{right} - \dot{m}r\omega_{right}}\right) \tag{29}$$

$$T(s) - Gv(s) = \left(\frac{M_{motor}}{2r} - (T_2 - T_1) - \dot{m}r\omega_{right}\right) \times e^{\mu\theta_{slip,right,ascend}} \tag{30}$$

By combining (16) with (30) and assuming $Y = \frac{M_{motor}}{2r} - (T_2 - T_1) - \dot{m}r\omega_{right}$, tension can be formulated as

$$T(s) = \left[Y + \frac{\dot{m}r\omega_{right}Y}{(Y+k)}\right]e^{\mu(s/r)} + \frac{\dot{m}r\omega_{right}k}{(Y+k)}. \tag{31}$$

C. TENSION ACTING ON THE PULLEY WHILE DESCENDING

The torque transferred to both the pulleys reverses the direction of the motor, thereby yielding the following equations:

$$T_{left} = \frac{M_{motor}}{2r} + (T_3 - T_2), \tag{32}$$

$$T_{right} = \frac{M_{motor}}{2r} + (T_2 - T_1). \tag{33}$$

Combining (8) with (32) and (33)

$$T_{left} = \frac{M_{motor}}{2r} + (T_3 - T_2) = k\left(\frac{r\omega_{left}}{v_{ref}} - 1\right) \tag{34}$$

$$T_{right} = \frac{M_{motor}}{2r} + (T_2 - T_1) = k\left(\frac{r\omega_{right}}{v_{ref}} - 1\right) \tag{35}$$

$$v_{ref} = k\left(\frac{r\omega_{left}}{\frac{M_{motor}}{2r} + (T_3 - T_2) + k}\right) \tag{36}$$

$$v_{ref} = k\left(\frac{r\omega_{right}}{\frac{M_{motor}}{2r} + (T_2 - T_1) + k}\right) \tag{37}$$

$$T\,(\mathrm{s}) = \left(\frac{v\,(s)}{r\omega_{left}}\left(\frac{M_{motor}}{2r} + (T_3 - T_2) + k\right) - k\right) \tag{38}$$

$$T\,(\mathrm{s}) = \left(\frac{v\,(s)}{r\omega_{right}}\left(\frac{M_{motor}}{2r} + (T_2 - T_1) + k\right) - k\right) \tag{39}$$

Similar to the previous ascending case, the final tension formula for the slip zone while descending is developed as follows.

1) SLIP ZONE OF THE LEFT PULLEY

Assuming $Z = \frac{M_{motor}}{2r} + (T_3 - T_2) - \dot{m}r\omega_{left}$,

$$T\,(s) = \left[Z + \frac{\dot{m}r\omega_{left}Z}{(Z+k)}\right]e^{-\mu(s/r)} + \frac{\dot{m}r\omega_{left}k}{(Z+k)}. \tag{40}$$

2) SLIP ZONE OF THE RIGHT PULLEY

Assuming $W = \frac{M_{motor}}{2r} + (T_2 - T_1) - \dot{m}r\omega_{right}$,

$$T\,(s) = \left[W + \frac{\dot{m}r\omega_{right}W}{(W+k)}\right]e^{-\mu(s/r)} + \frac{\dot{m}r\omega_{right}k}{(W+k)}. \tag{41}$$

D. ROPE DEFORMATION ACCORDING TO SLIP

The slip error can be obtained using Hooke's Law and the tension formula:

$$\varepsilon = \frac{T}{EA}, \tag{42}$$

$$d\delta_{slip} = \varepsilon r d\theta = \frac{1}{EA}\int_0^s T(s)ds, \tag{43}$$

$$\delta_{slip} = \delta_{slip,ascend} + \delta_{slip,descend}. \tag{44}$$

Because the rope is deformed by the tension difference in the slip zone, the position error due to the slip can be calculated by integrating the tension formula and the slip zone distance obtained above. This enables us to predict the position error during ascent and descent, respectively.

III. ROBUST EXPERIMENT DESIGN USING TAGUCHI METHOD

A. PROBLEM DEFINITION

The study aimed to increase the position accuracy of an FCR. In the previous section, the position error was predicted using several equations. However, the position accuracy could decrease if the position error compensation is performed without securing position repeatability. Therefore, position repeatability should be ensured first.

Position repeatability optimization of a rope winch was conducted using the Taguchi method. It is an experimental optimization technique.

The Taguchi method is a technique for improving product quality and designing products that are robust to noise factors that cannot be controlled. The Taguchi method involves system design, parameter design, and tolerance design procedures. The key is parameter design, which is a product engineering method that focuses on determining parameters and achieving the best quality characteristics with minimal variation. Unlike design of experiment, the Taguchi method can be utilized conveniently by users with limited knowledge of statistics.

Taguchi defined the S/N ratio as a quality characteristic of choice. It is used as a measurable value rather than a standard deviation. Its characteristics are divided into three categories:

nominal-the-best characteristic:

$$S/N = 10log\left(\frac{\bar{y}}{s_y^2}\right)$$

smaller-the-better characteristics:

$$S/N = -10\log\frac{1}{n}\left(\sum y^2\right)$$

larger-the-better characteristics:

$$S/N = -10\log\frac{1}{n}\left(\sum\frac{1}{y^2}\right),$$

where $\bar{y}$ is the average of the observed data, s_y^2 is the variance of y, n is the number of observations, and y is the observed data. For each type of characteristic, with the above S/N ratio transformation, the higher the S/N ratio, the better is the result [20], [21].

The Taguchi method is an experimental design using a special design of orthogonal arrays. It can study entire cases with a reduced number of experiments. The method has three main advantages: it can dramatically reduce the number of experiments, increase R&D productivity, and be applied to various fields.

The experiment was performed by the following steps: (Step 1) Select the objective function to be optimized. (Step 2) Identify the user condition and design parameters that affect the objective function, and select the levels of these factors. (Step 3) Select the orthogonal array. (Step 4) Assign design variables to the columns of the array. (Step 5) Perform experiments. (Step 6) Carry out S/N analysis on the results. (Step 7) Determine the optimal design parameters [22].

B. DEFINITION OF OBJECTIVE FUNCTION, DESIGN PARAMETERS, USER CONDITIONS, AND S/N RATIO

The position error (x_{ij}) at a point is defined as follows:

$$x_{ij} = P_{ij} - P_i \tag{45}$$

where P_{ij} represents the actual position and P_i represents the target position. Because this experiment aimed to minimize the positioning error of the rope winch, the objective function (y) was defined as the position error standard deviation.

$$y = \sqrt{\frac{1}{n-1}\sum_{j=1}^{n}\left(x_{ij} - \bar{x}_i\right)^2}, \tag{46}$$

where $\bar{x}_i$ represents the average of the position error at each target point and n represents the experiment cycle.

The experiments were performed under the following user conditions (Table 1) and design parameters (Table 2). Because the weight, motor velocity, and acceleration were difficult to control for robot operation, these were selected as the user conditions and divided into two levels: Levels 1 and 2 were classified as favorable and unfavorable conditions, respectively, for operation.

The pressure module force is important for producing a sufficient frictional force between the synthetic fiber rope and pulley. The problem is that although this force can help exert adequate frictional forces, it can also act as a resistance force owing to the radial elasticity of the rope [15]. Therefore, the number of pressure modules and the pressure module force were selected as design parameters because these could affect the position repeatability of the rope winch owing to the rope's characteristics.

TABLE 1. User conditions of the rope winch.

User Condition	Level 1		Level 2	
	N_1	N_2	N_3	N_4
Weight	60 kg	60 kg	10 kg	10 kg
Motor Velocity	2,000 rpm	2,000 rpm	5,000 rpm	5,000 rpm
Motor Acceleration	1,000 rpm/s	1,000 rpm/s	6,000 rpm/s	6,000 rpm/s
Direction	Ascending	Descending	Ascending	Descending

TABLE 2. Design parameters of first experiment.

Symbol	Design Parameters	Level 1	Level 2	Level 3
x_1	Number of Pressure Modules (Ea.)	1	2	-
x_2	Axial Direction Groove Pitch Angle (°)	4	5	6
x_3	Pressure Module Force (N)	30	45	60

In addition, in the previous research, the authors verified that the friction coefficient varies depending on the axial direction groove pitch angle of the pulley [16]. However, it was necessary to extend examination to the range left unexplored in the previous study, to verify whether the optimal friction coefficient exists in this range or not. Therefore, the axial direction groove pitch angle of the pulley was set as a design parameter.

Thus, the number of pressure modules (Fig. 4), axial direction groove pitch angle of the pulley (Fig. 5), and pressure module force (Fig. 6) were selected as the design parameters.

The number of pressure modules was set to one and two because the number of pulleys in the rope winch is designed for dual pulley and the pressure module can be mounted on each pulley.

The pressure module force was selected through preliminary experiments. It yielded insufficient frictional force in the range below 30 N (resulting in spin without traction) and limited rope movement in the range above 60 N. Therefore, 30 and 60 N were selected as the upper and lower values, respectively, and 45 N was selected as the middle value.

A previous study utilized groove pitch angles of 6°, 10°, and 18° [16]. The angle of 4°, 5°, and 6° were investigated in the first robust optimal design experiment and 6°, 8°, and 9° in the second experiment.

Because a two-level design parameter (number of pressure modules) and two three-level design parameters (axial direction groove pitch angle and pressure module force) were defined, the L_{18} ($2^1 \times 3^7$) Taguchi orthogonal array was selected.

Furthermore, the position error standard deviation was aimed to be minimized and the smaller-the-better S/N ratio was chosen as follows:

$$\text{S/N ratio} = -10\,log\left|\frac{(y_1)^2 + (y_2)^2 + \cdots + (y_n)^2}{n}\right| \quad (47)$$

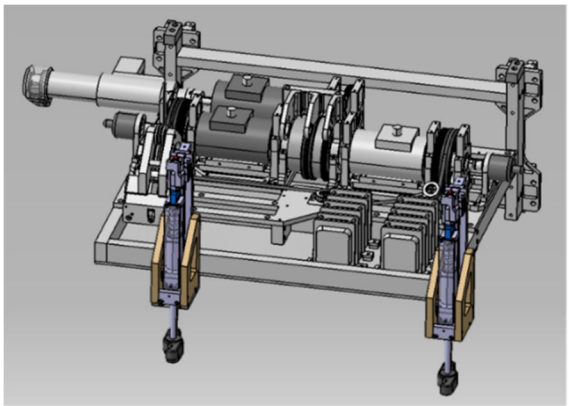

FIGURE 4. Pressure module location.

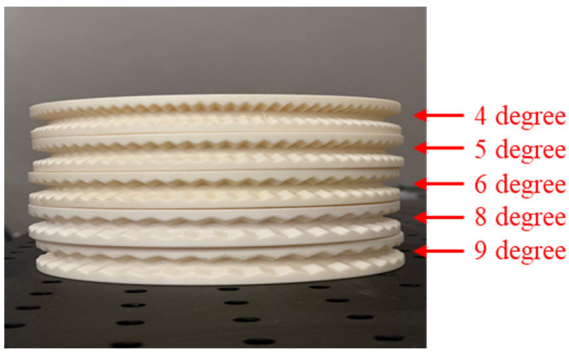

FIGURE 5. Pulleys with various axial groove pitch angles.

C. TEST BENCH AND EXPERIMENTAL METHOD

The experiment was conducted on a test bench, which comprises a mechanism identical to that of the rope winch

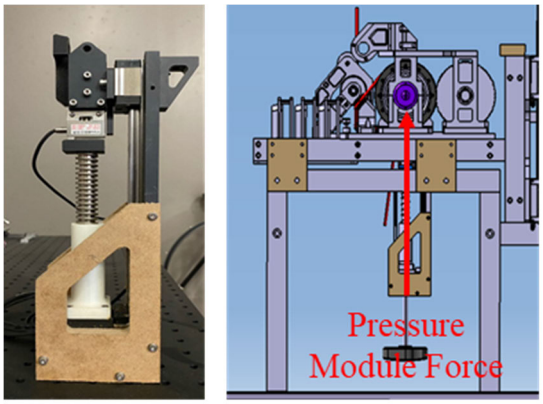

FIGURE 6. (Left) Pressure module and (Right) representation of the force.

mounted on the robot. It consists of three sections: the weight module, rope winch module, and test bench, as shown in Fig.7. In the rope winch module, a DC servo motor (Maxon, RE50, 200 W) was employed to deliver power to the differential gear module. The differential gear distributes power equally to both the pulleys. In addition, weight can be added to the weight module, and it moves upward and downward along the two linear guides on the test bench (Fig.7). This movement is considered as the robot's locomotion.

A magnetic linear encoder was installed and attached vertically to the test bench (resolution: 0.02 mm) to accurately measure the position of the weight module (Fig.8). International Organization for Standardization (ISO) specifications were employed to measure position repeatability as shown in Fig. 9 [23]. Furthermore, the travel distance to 3.0 m, 0.5 m per session was set because the height of a floor of the buildings is assumed to be 3.0m and to check the position error when the robot moves to one floor [24]. The position errors at five designated locations were measured, and each experiment was conducted five times. A synthetic fiber rope (nylon, diameter = 6 mm) was used for locomotion in this experiment. It is widely used in daily life.

D. TEST RESULTS OF THE FIRST EXPERIMENT

The results of the first experiment are summarized in Table 3. The position error standard deviation (position repeatability) and S/N ratio were calculated using (46) and (47), respectively.

The larger the S/N ratio, the more robust it is to variations in design parameters. This implies that the larger the S/N ratio, the better is the position repeatability. Furthermore, the variation in position repeatability is marginal even with variations in design parameters.

As shown in Table 3, Experiment 8 (one pressure module, an axial direction groove pitch of 6°, and a pressure module force of 45 N) is optimal for position repeatability because the S/N ratio is the highest.

The sensitivity analysis graph in Fig. 10 shows the highest S/N ratio for one pressure module, an axial direction groove pitch angle of 6°, and a pressure module force of 45 N.

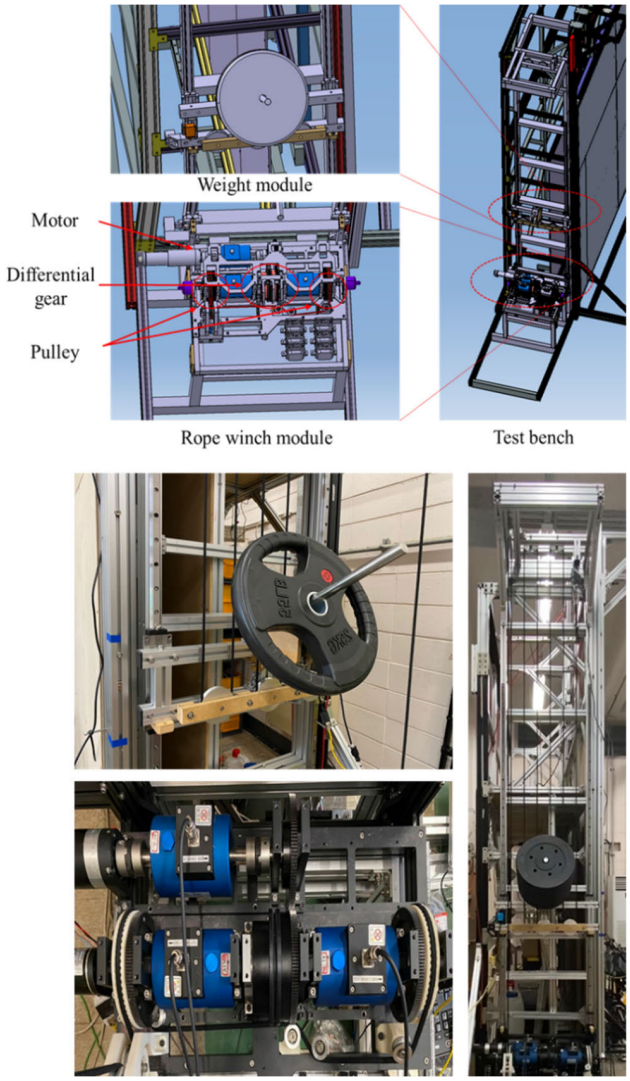

FIGURE 7. (Top) 3D model of the test bench and (Bottom) the actual test bench.

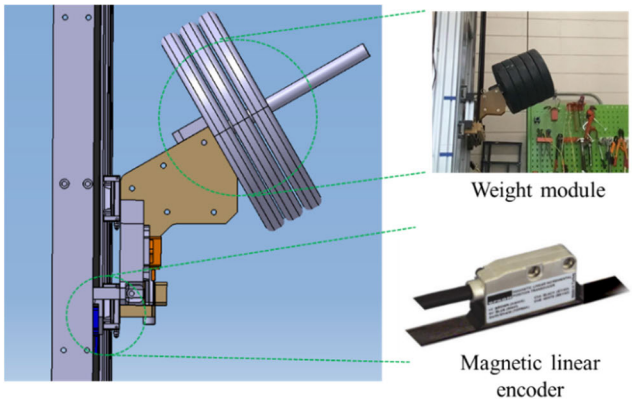

FIGURE 8. Weight module and magnetic linear encoder on the test bench.

These results show that the combination of design parameters with the highest S/N ratio (Experiment 8) matched that of design parameters with the highest S/N ratio in the sensitivity

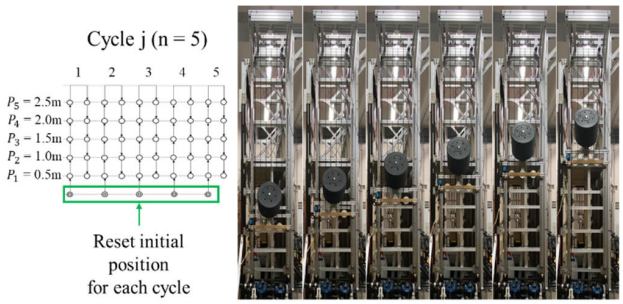

FIGURE 9. Method for measuring position repeatability (refer to ISO specification).

analysis. Thus, experiment 8 presents the best parameter combination for position repeatability tentatively.

TABLE 3. Test results of the first experiment.

Exp. Number	Design Parameter Level			Repeatability under User Conditions N_1, N_2, N_3, and N_4				S/N Ratio [dB]
	x_1	x_2	x_3	y_{N_1}	y_{N_2}	y_{N_3}	y_{N_4}	
1	1	1	1	0.319	0.507	0.358	0.480	7.46
2	1	1	2	0.273	0.352	0.362	0.418	9.00
3	1	1	3	0.211	0.417	0.360	0.381	9.09
4	1	2	1	0.362	0.535	0.426	0.478	6.84
5	1	2	2	0.152	0.407	0.267	0.351	10.18
6	1	2	3	0.362	0.453	0.241	0.386	8.67
7	1	3	1	0.229	0.273	0.263	0.320	11.27
8	1	3	2	0.085	0.102	0.224	0.290	14.21
9	1	3	3	0.116	0.078	0.509	0.760	6.69
10	2	1	1	0.469	0.742	0.751	0.842	2.92
11	2	1	2	0.246	0.413	0.283	0.416	9.18
12	2	1	3	0.098	0.121	0.439	0.501	9.32
13	2	2	1	0.112	0.133	0.439	0.646	7.95
14	2	2	2	0.329	0.619	0.336	0.404	7.17
15	2	2	3	0.258	0.290	0.440	0.497	8.30
16	2	3	1	0.141	0.310	0.626	0.641	6.39
17	2	3	2	0.279	0.347	0.323	0.430	9.14
18	2	3	3	0.319	0.358	0.408	0.392	8.63

As is evident from the sensitivity analysis results, the peripheral values of the design parameters could be investigated further because the S/N ratio may be higher at the peripheral values. Because the number of pressure modules installed is according to the number of pulleys, it could not be varied. Therefore, only one unit was utilized. Because the S/N ratio of the axial direction groove pitch angle increases with the angle, further investigations at higher pitch angles of 6°, 8°, and 9° were conducted. In addition, because the force of the pressure module is the highest point at 45 N, the peripheral values could be verified further. The values selected were 37.5, 45, and 52.5 N.

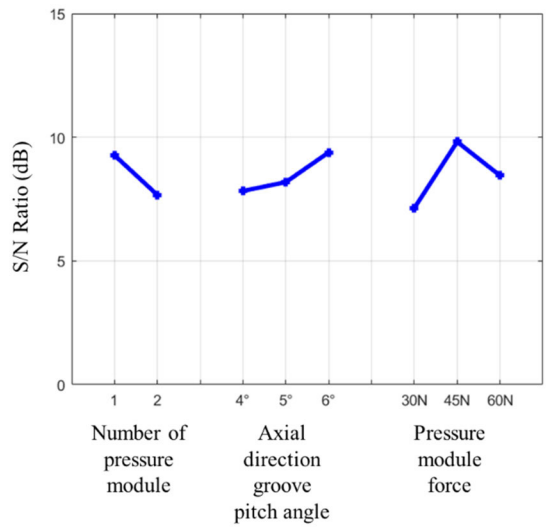

FIGURE 10. Sensitivity analysis of the first experiment.

E. TEST RESULTS OF THE SECOND EXPERIMENT

The newly determined design parameters are summarized in Table 4, and the results of the second experiment are shown in Table 5.

The experiment displayed the highest S/N ratio at a groove pitch angle of 6° and pressure module force of 45 N (Experiment 2 in Table 5). The above combination also had the highest S/N ratio in the results of both experiment and sensitivity analysis (see Fig. 11).

TABLE 4. Design parameters of second experiment.

Symbol	Design Parameters	Level 1	Level 2	Level 3
x_1'	Axial Direction Groove Pitch Angle (°)	6	8	9
x_2'	Pressure Module Force (N)	37.5	45	52.5

Therefore, it was concluded that a pressure module, an axial groove pitch angle of 6°, and a pressure module force of 45 N resulted in the best position repeatability. The position error can be compensated for with high precision using these rope winch design parameter values (which yield optimal position repeatability).

IV. POSITION ERROR COMPENSATION

A. POSITION ERROR COMPENSATION EXPERIMENTS

This chapter describes experiments that were conducted to verify the accuracy of the position error prediction model illustrated in Section II.

Feedforward control was used to evaluate the performance of the error prediction model for various weight ranges and travel distances because it can compensate for the error rapidly. PI controller was adopted to compensate for the additional position errors because it is one of the widely used and verified. For the synthetic fiber rope that because it has

TABLE 5. Test results of the second experiment.

Exp. Number	Design Parameter Level		Repeatability under User Conditions N_1, N_2, N_3, and N_4				S/N Ratio [dB]
	x_1'	x_2'	y_{N_1}'	y_{N_2}'	y_{N_3}'	y_{N_4}'	
1	1	1	0.274	0.268	0.418	0.426	9.01
2	1	2	0.140	0.076	0.139	0.246	15.79
3	1	3	0.187	0.186	0.257	0.335	12.07
4	2	1	0.377	0.556	0.327	0.379	7.56
5	2	2	0.231	0.204	0.258	0.195	13.02
6	2	3	0.268	0.330	0.373	0.478	8.63
7	3	1	0.562	0.894	0.724	0.846	2.30
8	3	2	0.484	0.425	0.233	0.341	8.35
9	3	3	0.299	0.707	0.219	0.268	7.52

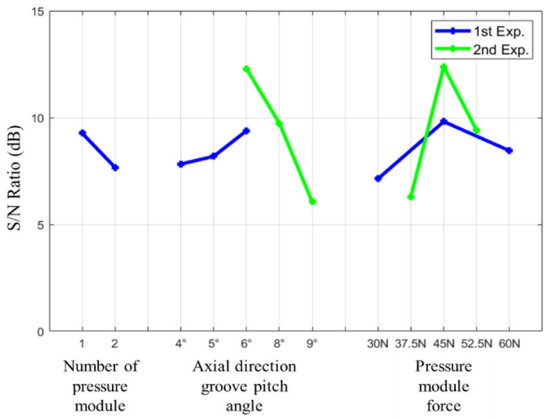

FIGURE 11. Sensitivity analysis of first and second experiments.

a low modulus of elasticity, sufficient time is required to reflect the motor's input in the robot's position. If the motor responds rapidly, unforeseen vibrations may occur while controlling the robot's position. Therefore, the derivative control for improving a rapidly varying response, such as overshoot, is not effective [24].

Similar test bench and methods were used for the position error compensation experiment (Figs. 8 and 9). The position error was measured at five locations. A DC servo motor (Maxon, RE50, 200 W) was used for the locomotion, and a motor driver (EPOS70/10) was used to control it. In addition, the experiment was conducted at Level 1 of Table 1 (motor velocity = 2000 rpm, motor acceleration = 1000 rpm/s), which is classified as a favorable condition.

The position input of the motor was measured using the rotary encoder attached to the motor. The actual position was measured using the magnetic linear encoder attached to the test bench.

B. POSITION ERROR DEFINITION

Position error is defined as 1) the deformation of the rope at the slip zone and 2) the backlash at the direction turnover. The tension of the rope and slip zone deformation error were predicted in the previous section. Therefore, the position error (x_{error}) is defined as the sum of the slip zone deformation error (δ_{slip}) and backlash term ($\delta_{backlash}$).

$$x_{error} = \delta_{slip} + \delta_{backlash} \tag{48}$$

C. ROPE MODULUS OF ELASTICITY MEASUREMENT

The rope modulus of elasticity should be predicted to calculate the slip error. A device to measure rope modulus of elasticity was designed and fabricated. Furthermore, a deformation test was performed as shown in Fig. 12.

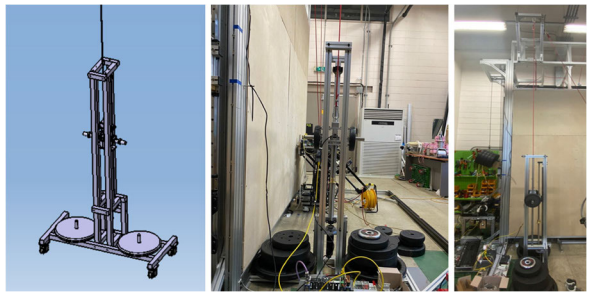

FIGURE 12. Device for measuring rope modulus of elasticity.

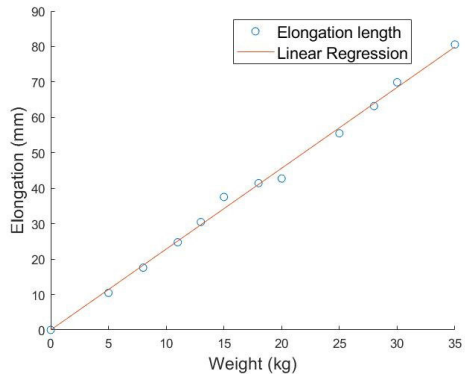

FIGURE 13. Elongation of the synthetic fiber rope.

The rope was fixed to the top of the test bench, and weights were added to the side of the device. The deformation was measured by a magnetic linear encoder (resolution = 0.02 mm).

The initial position of the device was fixed at the reference position, and weights ranging from 5 to 35 kg were added. The deformation results are presented in Fig. 13 and Table 6. As shown in Fig. 13, the rope modulus of elasticity appears to be linear and is calculated using the measured figures.

It should be noted that the elongation length was measured during 60 s of loading because the synthetic fiber rope was influenced by time. The modulus of elasticity of the rope was calculated as 4.0×10^8 Pa using Hooke's law:

$$E = \frac{TL}{\delta_{elongation} A} \tag{49}$$

TABLE 6. Rope elongation measurement results.

Applied weight (kg)	Elongation length (mm)	Modulus of Elasticity (Pa × 10^8)
5	10.5	4.3
8	17.6	4.1
11	24.8	4.0
13	30.5	3.8
15	37.5	3.6
18	41.4	3.9
20	42.7	4.2
25	55.5	4.0
28	63.2	4.0
30	69.9	3.9
35	80.6	3.9

TABLE 7. Backlash measurement results.

Exp. Number	P_6	P_5	P_4	Backlash (m)
1	0.509	0.011	-0.507	0.019
2	0.509	0.011	-0.507	0.020
3	0.509	0.010	-0.507	0.019
4	0.508	0.011	-0.507	0.021
5	0.508	0.011	-0.508	0.021
6	0.508	0.010	-0.509	0.020
7	0.507	0.009	-0.510	0.020
8	0.508	0.009	-0.510	0.021
9	0.508	0.009	-0.509	0.020
10	0.508	0.009	-0.510	0.020

D. BACKLASH MEASUREMENT

Backlash occurs when the movement direction varies from ascent to descent, and vice versa. The backlash was measured experimentally. The top three points were selected, and the movement distance was measured when turnover occurred as in Fig. 14. The backlash formula is as follows:

$$\delta_{backlash} = (P_5 - P_4) - (P_6 - P_5) \tag{50}$$

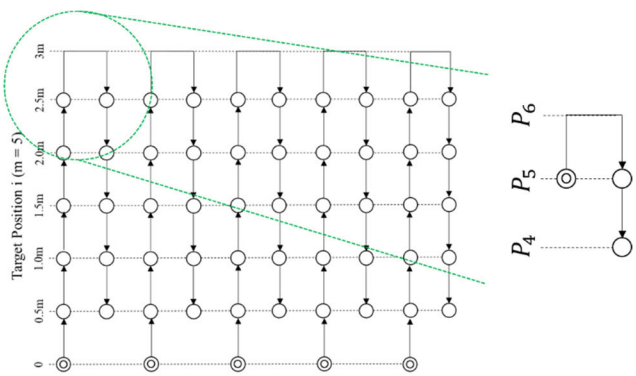

FIGURE 14. Schematics of backlash measurement.

The backlash was determined to be 0.02 m (mean value of 10 measurements).

E. CONTROL STRUCTURE OF POSITION ERROR COMPENSATION

The position error was compensated through open-loop, feedforward, and feedforward + PI control (Fig. 15). The experiments were performed with loads of 60, 70, and 80 kg on the rope winch, and travel distances of 1.5, 3.0, and 4.5 m. The ramp profile (which moves 1.5 m at 0.25 m intervals, 3.0 m at 0.5 m intervals, and 4.5 m at 0.75 m intervals) was entered as the desired position input (x_d).

Only x_d was input into the motor driver for open-loop. In the case of feedforward control, the error values were entered using the error prediction model, and the backlash values were entered while switching directions at the highest point. The feedforward input is $x_f = x_{error} = \delta_{slip} + \delta_{backlash}$. Here, δ_{slip} is defined as $\frac{1}{EA}\int_0^S T(s)ds$ in Eq. (43). The $T(s)$ during ascent is as illustrated in (24) and (31), and that during descent is as illustrated in (40) and (41).

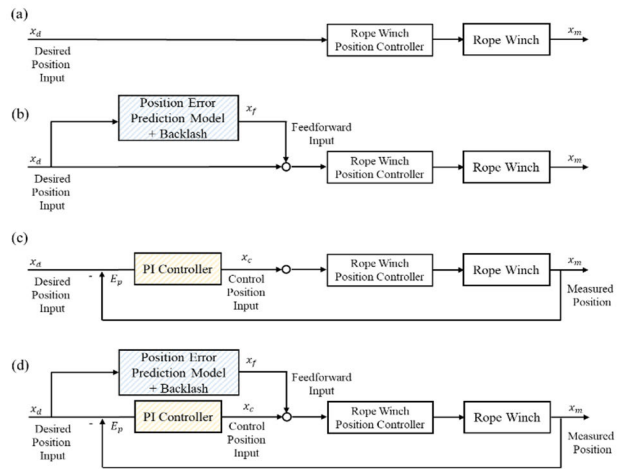

FIGURE 15. Block diagrams of open-loop (a), feedforward control (b), PI control (c), and feedforward + PI (d) control plans.

The backlash and modulus of elasticity of the rope were measured experimentally as described in the previous chapter and applied to feedforward. It is infeasible to accurately predict the slip zone length because it is challenging to detect using sensors. Therefore, the optimal value of the slip zone was determined through experiments.

When PI and feedforward + PI control were conducted, the position difference between the actual and desired positions was measured by the linear encoder and reflected in the feedback loop.

F. POSITION ERROR COMPENSATION RESULT AND DISCUSSION

The position trajectories of rope winch and position error compensation results are shown in Fig16-18 and Tables 8–10. In the case of feedforward control results for a travel distance of 3.0 m (Fig. 16, Table 8), the use of an error prediction model can reduce the positioning error of rope winch to 56%–81% in terms of the mean of absolute value and 55%–76% based on the RMS value. The position errors of mean absolute values were 10–16 mm and the RMS values were 15–20 mm; these accounted for 0.3%–0.5% and 0.5%–0.7% of the values, respectively. Meanwhile, in the absence of compensation, the mean absolute value was 25–53 mm, and the RMS value was 38–63 mm. These accounted for 0.8%–1.8% and 1.3%–2.1% respectively.

Experiments on PI control and feedforward + PI control were also performed. PI controller can reduce position error of rope winch to 56%–79% in terms of the mean of absolute value and 55%–70% in terms of the RMS value. The position error of mean absolute values was 11-12mm and the RMS values were 17-19mm out of 3.0m and these accounted for 0.4% and 0.6% respectively.

TABLE 8. Position error comparison among Open-loop, Feedforward, PI, and Feedforward + PI controller for travel distance 3.0m at 0.5m interval.

Weight	Position Error (mm) Mean of absolute value			
	Open-loop	Feedforward	PI	Feedforward + PI
60kg	25	11 (↓ 56%)	11 (↓ 56%)	7 (↓ 72%)
70kg	44	16 (↓ 64%)	12 (↓ 73%)	6 (↓ 86%)
80kg	53	10 (↓ 81%)	11 (↓ 79%)	6 (↓ 89%)
Weight	Position Error (mm) RMS Value			
	Open-loop	Feedforward	PI	Feedforward + PI
60kg	38	17 (↓ 55%)	17 (↓ 55%)	10 (↓ 74%)
70kg	55	20 (↓ 64%)	19 (↓ 65%)	9 (↓ 84%)
80kg	63	15 (↓ 76%)	19 (↓ 70%)	9 (↓ 86%)

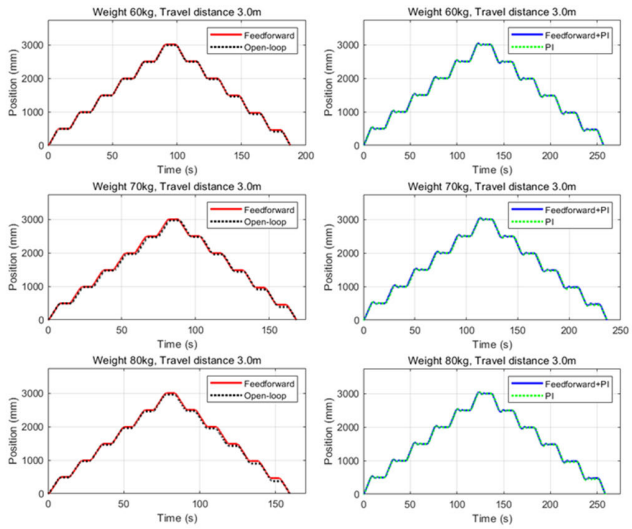

FIGURE 16. Position trajectories of rope winch with weights and controllers for travel distance 3.0m at 0.5m interval.

Feedforward + PI controller can reduce the positioning error of a rope winch to 72%–89% in terms of the mean of absolute value and 74%–86% based on RMS value. The position errors of mean absolute values were 6–7 mm and the RMS values were 9–10 mm. These accounted for 0.2% and 0.3% respectively.

Whether it is open-loop or PI control, the position error is further reduced when feedforward control is added. These outcomes show that employing feedforward help to reduce position error and explain why the feedforward control method is essential for robot locomotion.

Because robot positions in scenarios where the robot moves vertically were focused, comparative experiments were conducted on the various distances to resolve the uncertainty over these distances.

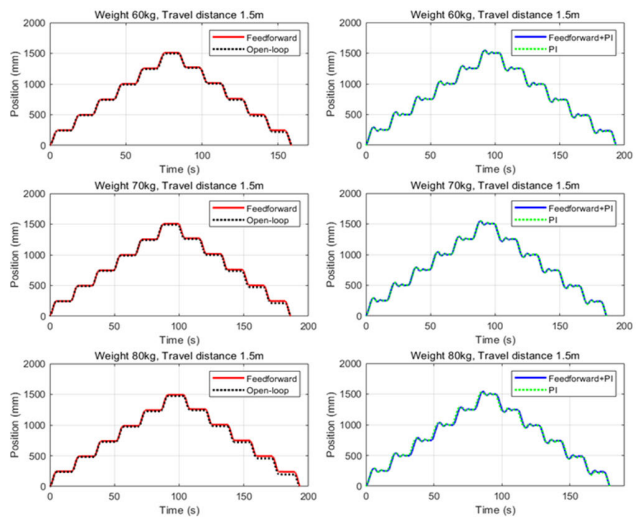

FIGURE 17. Position trajectories of rope winch with weights and controllers for travel distance 1.5m at 0.25m interval.

In the case of feedforward control results for a travel distance of 1.5 m (Fig.17, Table 9), the use of an error prediction model can reduce the positioning error of rope winch to 36%–70% in terms of the mean of absolute value and 23%–70% based on the RMS value. The position errors of mean absolute values were 6–8 mm and the RMS values were 9–10 mm; these accounted for 0.4%–0.5% and 0.6%–0.7% respectively. Meanwhile, in the absence of compensation, the mean absolute value was 11–27 mm, and the RMS

value was 13–30 mm. These accounted for 0.7%–1.8% and 0.9%–2.0% respectively.

TABLE 9. Position error comparison among Open-loop, Feedforward, PI, and Feedforward + PI controller for travel distance 1.5m at 0.25m interval.

Weight	Position Error (mm) Mean of absolute value			
	Open-loop	Feedforward	PI	Feedforward + PI
60kg	11	7 (↓36%)	5 (↓55%)	4 (↓64%)
70kg	13	6 (↓54%)	5 (↓62%)	3 (↓77%)
80kg	27	8 (↓70%)	9 (↓67%)	7 (↓74%)
Weight	Position Error (mm) RMS Value			
	Open-loop	Feedforward	PI	Feedforward + PI
60kg	13	10 (↓23%)	9 (↓31%)	5 (↓61%)
70kg	17	9 (↓47%)	7 (↓59%)	4 (↓76%)
80kg	30	9 (↓70%)	13 (↓57%)	8 (↓74%)

PI controller can reduce position error of rope winch to 55%–67% in terms of the mean of absolute value and 31%–59% in terms of the RMS value. The position error of mean absolute values was 5-9mm and RMS values were 7-13mm and these accounted for 0.3%-0.6% and 0.5%-0.9% respectively.

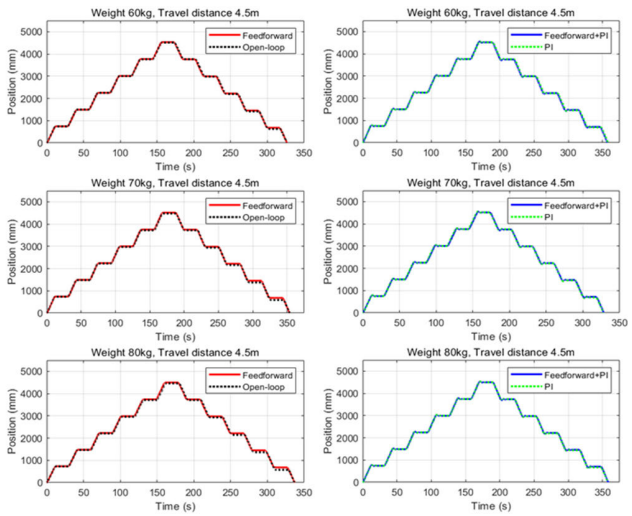

FIGURE 18. Position trajectories of rope winch with weights and controllers for travel distance 4.5m at 0.75m interval.

Feedforward + PI controller can reduce the positioning error of a rope winch to 64%–77% in terms of the mean of absolute value and 61%–76% based on RMS value. The position errors of mean absolute values were 3–7 mm and the

TABLE 10. Position error comparison among Open-loop, Feedforward, PI, and Feedforward + PI controller for travel distance 4.5m at 0.75m interval.

Weight	Position Error (mm) Mean of absolute value			
	Open-loop	Feedforward	PI	Feedforward + PI
60kg	31	20 (↓35%)	18 (↓42%)	12 (↓61%)
70kg	56	19 (↓66%)	17 (↓70%)	10 (↓82%)
80kg	69	27 (↓61%)	25 (↓64%)	19 (↓72%)
Weight	Position Error (mm) RMS Value			
	Open-loop	Feedforward	PI	Feedforward + PI
60kg	49	29 (↓41%)	25 (↓49%)	17 (↓65%)
70kg	75	28 (↓63%)	25 (↓67%)	15 (↓80%)
80kg	85	32 (↓62%)	35 (↓59%)	23 (↓73%)

RMS values were 4–8 mm. These accounted for 0.2-0.5% and 0.3-0.5% respectively.

In the case of feedforward control results for a travel distance of 4.5 m (Fig. 18, Table 10), the use of an error prediction model can reduce the positioning error of rope winch to 35%–66% in terms of the mean of absolute value and 41%–63% based on the RMS value. The position errors of mean absolute values were 19–27 mm and the RMS values were 28–32 mm; these accounted for 0.4%–0.6% and 0.6%–0.7% respectively. Meanwhile, in the absence of compensation, the mean absolute value was 31–69 mm, and the RMS value was 49–85 mm. These accounted for 0.7%–1.5% and 1.1%–1.9% respectively.

PI controller can reduce position error of rope winch to 42–70% in terms of the mean of absolute value and 49–67% in terms of the RMS value. The position error of mean absolute values was 17-25mm and the RMS values were 25-35mm and these accounted for 0.4%-0.6% and 0.6%-0.8% respectively.

Feedforward + PI controller can reduce the positioning error of a rope winch to 61%–82% in terms of the mean of absolute value and 65%–80% based on RMS value. The position errors of mean absolute values were 10–19 mm and the RMS values were 15–23 mm. These accounted for 0.2%-0.4% and 0.3%-0.5% respectively.

Thus, an error compensation model is effective even when the travel distance is increased or decreased. The overall results show that the position accuracy was the highest when the feedforward + PI controller was used, from among the three control plans.

It is noteworthy that using only PI control is worse than using feedforward control at the load of 80kg. This is because

when using PI control, additional backlash errors might be caused by repeated rise and fall of the rope winch during convergence, and additional slipping might be caused due to lack of friction force as the weight increases.

The additional experiments were also showed that employing a feedforward controller help to reduce position error significantly and explain why the feedforward control method is essential for robot whether the travel distance increases or decreases.

Position errors are dominant during descent rather than ascent. Thus, higher compensation is required during the former. It is noteworthy that the error tends to be compensated well as the weight increases. This is because the elasticity of the rope could affect the position. Other error factors may include the fact that the dynamic characteristics were not considered because the vibration of the rope was observed during the experiment. Although the elastic modulus of the rope was assumed to be linear, the tensile values of the rope varied over time. These must be considered in future research.

In the previous research, the rope elongation property is assumed to be non-linear and the error prediction modeling is complicated [19]. However, the rope property was assumed to be linear and the error modeling is relatively simple in this research, resulting in similar or even better position error compensation results. In addition, the position accuracy was much more improved by using feedforward + PI controller than using feedforward controller (Table 11).

TABLE 11. Position error percentage comparison OL: Open-Loop, FF: Feedforward.

Error	Controller	Travel distance of 10m at 2.0m interval [19]			Travel distance of 3.0m at 0.5m interval		
		88N	121N	154N	60kg	70kg	80kg
RMS	OL	1.5%	1.7%	2.0%	1.3%	1.8%	2.1%
	FF	0.4%	0.4%	0.8%	0.6%	0.7%	0.5%
	FF+PI	N/A			0.3%	0.3%	0.3%

V. CONCLUSION

This study aimed to improve the position accuracy of an MWDPW. Theoretical modeling for position error prediction was performed with this objective. The rope and pulley mechanics were verified using a free body diagram of the rope and pulleys. The rope was assumed to be elastic, and an equation for rope tension was derived. The slip zone was then predicted to verify the difference in tension of the rope wound around the pulleys, which can result in rope deformation and position errors.

To adequately compensate for the positional errors, position repeatability must be ensured. Therefore, empirical optimization was conducted using the Taguchi method, and the optimal position repeatability was verified through experiments. The case with a pressure module, an axial groove pitch angle of 6°, and pressure module force of 45 N exhibited the best position repeatability.

Because the position repeatability was secured, position error compensation was performed through feedforward and feedforward + PI control using error prediction model. The backlash and rope modulus of elasticity were measured experimentally. Using the above results, the position accuracies for 60, 70, and 80 kg and travel distances of 1.5, 3.0, and 4.5 m were verified experimentally, and the position errors before and after compensation were compared. The error in position improved by over 55%–81% through feedforward control and 72%–89% through feedforward + PI control, which corresponds to deviations of 0.3%–0.5% and 0.2-0.3%, respectively, of the overall 3.0 m movement. In the previous research, the rope deformation is assumed to be non-linear and the error modeling is complicated. However, the rope was assumed to be linear and the error modeling is relatively simple in this research, resulting in similar or even better position error compensation results. Therefore, this study contributes to the position error prediction and accuracy improvement of FCRs.

ACKNOWLEDGMENT

The authors deeply appreciate Kyungwook Lee, Myeongjin Choi, and Yecheol Moon of Robot Design Engineering Laboratory, Hanyang University for their contributions to the experiments carried out in this research. They would like to thank Editage (www.editage.co.kr) for English language editing.

REFERENCES

[1] D. Cortese. (Jul. 18, 2018). *What is a Skyscraper?*. THEB1M, London, U.K. Accessed: Aug. 4, 2021. [Online]. Available: https://www.theb1m.com/video/what-is-a-skyscraper

[2] S. Raga. (May 4, 2016). *13 Behind-the-Scenes Secrets of Professional Window Washers*. Mental Floss, New York City, NY, USA. Accessed: Aug. 4, 2021. [Online]. Available: https://www.mentalfloss.com/article/79507/13-behind-scenes-secrets-professional-window-washers

[3] T. Akinfiev, M. Armada, and S. Nabulsi, "Climbing cleaning robot for vertical surfaces," *Ind. Robot, Int. J.*, vol. 36, no. 4, pp. 352–357, Jun. 2009.

[4] N. Elkmann, M. Lucke, T. Krüger, D. Kunst, T. Stürze, and J. Hortig, "Kinematics, sensors and control of the fully automated Façade-cleaning robot SIRIUSc for the Fraunhofer headquarters building, Munich," *Ind. Robot, Int. J.*, vol. 35, no. 3, pp. 224–227, May 2008.

[5] E. Gambao and M. Hernando, "Control system for a semi-automatic Façade cleaning robot," in *Proc. 23rd Int. Symp. Autom. Robot. Construct.*, Oct. 2006, pp. 406–411.

[6] S. Moon, J. Huh, D. Hong, S. Lee, and C. Han, "Vertical motion control of building façade maintenance robot with built-in guide rail," *Robot. Comput.-Integr. Manuf.*, vol. 31, pp. 11–20, Feb. 2015

[7] Kite Robotics, Enschede, The Netherlands. *Kite Robotics Window Cleaning Robots*. Accessed: Aug. 4, 2021. [Online]. Available: https://www.kiterobotics.com

[8] N. Imaoka, S.-g. Roh, N. Yusuke, and S. Hirose, "SkyScraper-I: Tethered whole Windows cleaning robot," in *Proc. IEEE/RSJ Int. Conf. Intell. Robots Syst.*, Taipei, Taiwan, Oct. 2010, pp. 5460–5465, doi: 10.1109/IROS.2010.5649537.

[9] J. Hong, G. Park, J. Lee, J. Kim, H. S. Kim, and T. Seo, "Performance comparison of adaptive mechanisms of cleaning module to overcome step-shaped obstacles on Façades," *IEEE Access*, vol. 7, pp. 159879–159887, 2019.

[10] Wall Robotics, Espoo, Finland. *Full Self Cleaning Robot From Wall Robotics*. Accessed: Aug. 25, 2020. [Online]. Available: https://www.wallrobotic.com

[11] IPC Eagle, USA. *High Rise Professional Window Cleaning System*. Accessed: Jul. 20, 2021. [Online]. Available: http://www.ipcworldwide.com/us/product/highrise-automatic-window-cleaning-system/

[12] K. Seo, S. Cho, T. Kim, H. S. Kim, and J. Kim, "Design and stability analysis of a novel wall-climbing robotic platform (ROPE RIDE)," *Mechanism Mach. Theory*, vol. 70, pp. 189–208, Dec. 2013.

[13] M. S, Shafi, J. Lu, Z. Song, and Y. Fu, "Design and tension control of double drum winch system for deep-sea exploration equipment," in *Proc. 5th Int. Conf. Inf. Eng. Mech. Mater.*, Jul. 2015, pp. 1474–1480.

[14] S. R. Torben, P. Ingeberg, Ø. Bunes, S. Bull, J. Paterson, and D. Davidson, "Fiber rope deployment system for ultradeepwater installations," in *Proc. Offshore Technol. Conf.*, Apr. 2007, pp. 1–11.

[15] S. Yoo, T. Kim, M. Seo, J. Oh, J. Kim, H. S. Kim, and T. Seo, "Highly repeatable rope winch design with multiple windings and differential gear mechanism," *IEEE Access*, vol. 8, pp. 87291–87308, 2020.

[16] M. Choi, H. Chae, K. Kim, and T. Seo, "Robust design of a rope ascender based on geometric parameters of traction sheave," *Int. J. Precis. Eng. Manuf.*, vol. 22, no. 5, pp. 965–974, May 2021.

[17] S. Yoo, I. Joo, J. Hong, C. Park, J. Kim, H. S. Kim, and T. Seo, "Unmanned high-rise Façade cleaning robot implemented on a gondola: Field test on 000-building in Korea," *IEEE Access*, vol. 7, pp. 30174–30184, 2019.

[18] S. E. Bechtel, S. Vohra, K. I. Jacob, and C. D. Carlson, "The stretching and slipping of belts and fibers on pulleys," *J. Appl. Mech.*, vol. 67, no. 1, pp. 197–206, Mar. 2000.

[19] S. Yoo, T. Kim, M. Seo, J. Oh, J. Kim, H. S. Kim, and T. Seo, "Modeling and verification of multi-winding rope winch for facade operation," *Mechanism Mach. Theory*, vol. 155, Jan. 2021, Art. no. 104105.

[20] J. A. Ghani, I. A. Choudhury, and H. H. Hassan, "Application of Taguchi method in the optimization of end milling parameters," *J. Mater. Process. Technol.*, vol. 145, no. 1, pp. 84–92, Jan. 2004.

[21] S. K. Karna and R. Sahai, "An overview on Taguchi method," *Int. J. Eng. Math. Sci.*, vol. 1, no. 1, pp. 1–7, 2012.

[22] J. L. Rosa, A. Robin, M. B. Silva, C. A. Baldan, and M. P. Peres, "Electrodeposition of copper on titanium wires: Taguchi experimental design approach," *J. Mater. Process. Technol.*, vol. 209, no. 3, pp. 1181–1188, Feb. 2009.

[23] *Test Code for Machine Tools—Part 2: Determination of Accuracy and Repeatability of Positioning of Numerically Controlled Axes*, ISO Standard 230-2:2014, 2014.

[24] A. Guleria, "Structural analysis of a multi-storeyed building using ETABS for different plan configurations," *Int. J. Eng. Res. Technol.*, vol. 3, no. 5, pp. 1481–1485, May 2014.

[25] S. Yoo, T. Kim, M. Seo, J. Oh, H. S. Kim, and T. Seo, "Position-tracking control of dual-rope winch robot with rope slip compensation," *IEEE/ASME Trans. Mechtron.*, vol. 26, no. 4, pp. 1754–1762, Aug. 2021.

HONGJOON KYONG received the B.S. degree in mechanical engineering from Korea Aerospace University, in 2014. He is currently pursuing the M.S. degree in mechanical and aerospace engineering with Seoul National University. His research interests include robot mechanism design, modeling, and control.

MYEONGJIN CHOI received the B.S. degree in electronic engineering from Hanyang University, in 2020, where he is currently pursuing the M.S. degree in mechanical engineering. His research interests include robot mechanism design, control, and optimization.

YECHEOL MOON received the B.S. degree in mechanical engineering from Hanyang University, Seoul, South Korea, in 2018, and the M.S. degree from the Department of Mechanical Convergence Engineering, Hanyang University, in 2020, where he is currently pursuing the Ph.D. degree. His research interests include the design of new mechanisms and kinematic and dynamic control of robotic platforms.

KYUNGWOOK LEE received the B.S. degree in mechanical and control engineering from Handong Global University, Pohang, South Korea, in 2021. He is currently pursuing the M.S. degree in mechanical convergence engineering with Hanyang University, Seoul, South Korea. His research interest includes robot mechanism design.

JONGWON KIM received the B.S. degree in mechanical engineering from Seoul National University, South Korea, in 1978, the M.S. degree in mechanical and aerospace engineering from the Korea Advanced Institute of Science and Technology (KAIST), South Korea, in 1980, and the Ph.D. degree in mechanical engineering from the University of Wisconsin-Madison, USA, in 1987. He is currently a Professor with the School of Mechanical and Aerospace Engineering, Seoul National University. His current research interests include parallel mechanisms, Taguchi methodology, and field robots.

TAEGYUN KIM received the B.S. and Ph.D. degrees in mechanical and aerospace engineering from Seoul National University, South Korea, in 2011 and 2017, respectively. He was a Senior Engineer at the Mechatronics Research and Development Center, Samsung Electronics Company, from 2017 to 2019. He is currently an Assistant Professor with the School of Mechanical Engineering, Yeungnam University. His current research interests include robot mechanism design, robust control, and smart factory.

TAEWON SEO (Senior Member, IEEE) received the B.S. and Ph.D. degrees from the School of Mechanical and Aerospace Engineering, Seoul National University, South Korea. He is currently an Associate Professor with the School of Mechanical Engineering, Hanyang University, South Korea. Prior to this, he was a Postdoctoral Researcher at the Nanorobotics Laboratory, Carnegie Mellon University; a Visiting Professor at the Biomimetic Millisystems Laboratory, UC Berkeley; and an Assistant Professor at the School of Mechanical Engineering, Yeungnam University, South Korea. His research interests include robot design, analysis, control, optimization, and planning. He received the Best Mechatronics Paper Award of IEEE/ASME Transaction on Mechatronics, in 2014. He is working as a Technical Editor of IEEE/ASME Transactions on Mechatronics. He is an Associate Editor of IEEE Robotics and Automation Letters and *Intelligent Service Robotics*.